

Chapter 2

Power System Modelling and Analysis Techniques

Various well documented tools are available to engineers for power system modelling and analysis. This chapter will describe the fundamental techniques required to complete studies on the stability of power systems including HVDC systems. Within this chapter, models are presented for all of the main components of electrical power systems, including synchronous generators, excitation systems, power system stabilisers, power transformers, transmission lines, systems loads and the electrical network. The modelling technique used to handle the time delays associated with wide area signals is also given. Following this, the techniques used to represent the HVDC system for power system stability analysis are presented, including relevant control schemes and converter controllers. The methods of modelling HVDC lines and multi-terminal HVDC grids are also provided.

In addition to the modelling techniques presented, tools for power system stability analysis based on system linearisation are also described. Once this framework has been established, the damping controller designs utilised within this thesis are thoroughly discussed. Finally, a description of the various test networks used whilst completing this research is presented.

Throughout this thesis, all modelling has been completed using the MATLAB/Simulink environment (version 7.9.0, R2009b) with direct implementation of the mathematical component descriptions outlined within this chapter.

2.1 Modelling Power System Components

Within this section, the models of all main power system components are presented. These models have been used throughout the research to provide the simulation results presented later. The power system, and all included components, are modelled using an orthogonal phase representation, under the assumption that all three phases are balanced [1].

2.1.1 Synchronous Generators

The synchronous generator is the fundamental source of energy within modern electrical power networks, and can be modelled with varying levels of complexity. Two different synchronous generator models are used within this thesis, a sixth order model including leakage reactance, and a fifth order model neglecting leakage reactance.

2.1.1.1 Sixth Order Model with Leakage Reactance

The first order differential equations for the sixth order synchronous generator model including leakage reactance are given by (2.1–2.6) with notation consistent with [2].

$$\frac{d}{dt}E'_d = \frac{1}{T'_{qo}} \left[-E'_d + (X_q - X'_q) \left\{ I_q - \frac{X'_q - X''_q}{(X'_q - X_{lk,s})^2} (\psi_{2q} + (X'_q - X_{lk,s})I_q + E'_d) \right\} \right] \quad (2.1)$$

$$\frac{d}{dt}E'_q = \frac{1}{T'_{do}} \left[-E'_q - (X_d - X'_d) \left\{ I_d - \frac{X'_d - X''_d}{(X'_d - X_{lk,s})^2} (\psi_{1d} + (X'_d - X_{lk,s})I_d - E'_q) \right\} + E_{fd} \right] \quad (2.2)$$

$$\frac{d}{dt}\psi_{1d} = \frac{1}{T''_{do}} \left[-\psi_{1d} + E'_q - (X'_d - X_{lk,s})I_d \right] \quad (2.3)$$

$$\frac{d}{dt}\psi_{2q} = \frac{1}{T''_{qo}} \left[-\psi_{2q} - E'_d - (X'_q - X_{lk,s})I_q \right] \quad (2.4)$$

$$\frac{d}{dt}\Delta\omega_r = \frac{1}{2H} [P_m - P_e - D\Delta\omega_r] \quad (2.5)$$

$$\frac{d}{dt}\delta = (\omega_r - \omega_{syn}) = \Delta\omega_r \quad (2.6)$$

The algebraic equations defining the stator voltages and generator electrical real power are given by (2.7–2.10), assuming the generator armature resistance is negligible.

$$E_d = \frac{X''_q - X_{lk,s}}{X'_q - X_{lk,s}} E'_d - \frac{X'_q - X''_q}{X'_q - X_{lk,s}} \psi_{2q} + X''_q I_q \quad (2.7)$$

$$E_q = \frac{X_d'' - X_{lk,s}}{X_d' - X_{lk,s}} E_q' + \frac{X_d' - X_d''}{X_d' - X_{lk,s}} \psi_{1d} - X_d'' I_d \quad (2.8)$$

$$E_t = \sqrt{E_d^2 + E_q^2} \quad (2.9)$$

$$P_e = E_d I_d + E_q I_q \quad (2.10)$$

2.1.1.2 Fifth Order Model Neglecting Leakage Reactance

In the fifth order model it is assumed that $E_d' = 0$ and that $X_q' = X_q$. The leakage reactance is also neglected, resulting in the use of (2.11–2.13) for the generator voltage state equations and (2.5) and (2.6) representing the mechanical dynamics of the generator [1].

$$\frac{d}{dt} E_q' = \frac{1}{T_{do}''} \left[E_{fd} - E_q' + I_d (X_d - X_d') \right] \quad (2.11)$$

$$\frac{d}{dt} E_d'' = \frac{1}{T_{qo}''} \left[-E_d'' - I_q (X_q' - X_q'') \right] \quad (2.12)$$

$$\frac{d}{dt} E_q'' = \frac{1}{T_{do}''} \left[E_q' - E_q'' + I_d (X_d' - X_d'') \right] \quad (2.13)$$

The algebraic equations describing the d - and q -axis stator voltages are given as (2.14) and (2.15) with the generator stator terminal voltage and electrical power output defined as (2.9) and (2.10) respectively.

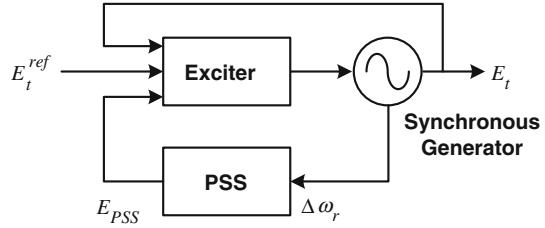
$$E_q = E_q'' - X_d'' I_d \quad (2.14)$$

$$E_d = E_d'' - X_q'' I_q \quad (2.15)$$

2.1.2 Generator Excitation Systems

Generators are reliant on excitation systems to provide direct current to the synchronous machine field winding [3]. Furthermore, through controlling the field voltage E_{fd} (and therefore the field current), the excitation system is able to contribute towards maintaining power system stability. This control is provided by the AVR, which manipulates the field voltage in order to reach the generator stator terminal voltage reference set-point, E_t^{ref} , and to ensure the *first-swing* stability of the machine. A power system stabiliser may also be included in order to reduce

Fig. 2.1 Relationship and signals between the synchronous generator, excitation system, and power system stabiliser



rotor speed variations following disturbances. The functional relationship between the synchronous generator, excitation system, and PSS (if included) is shown in Fig. 2.1.

Various excitation systems are used in practice, with comprehensive details found in [4]. Descriptions of the excitation systems used within this thesis are provided in the following sections.

2.1.2.1 Manual Excitation

Manual excitation is the simplest excitation scheme, with the field voltage E_{fd} maintained at a constant value determined during the synchronous generator parameter initialisation. No AVR is used and therefore the generator terminal voltage may vary from the desired value if operating conditions change.

2.1.2.2 Static Excitation (IEEE Type ST1A)

Static excitation systems supply direct current to the generator field winding through rectifiers which are fed by either transformers or auxiliary machine windings [4]. A simplified version of the IEEE Type ST1A static exciter is shown in Fig. 2.2, consisting of voltage transducer delay, exciter, and Transient Gain Reduction (TGR). The signal E_{PSS} is a stabilising signal from the PSS, if one is used in conjunction with the exciter.

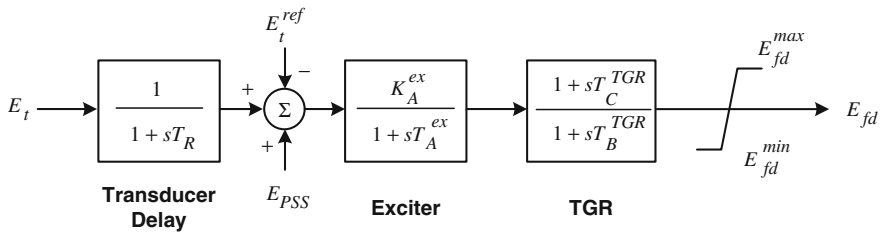


Fig. 2.2 Simplified block diagram for the IEEE Type ST1A static exciter

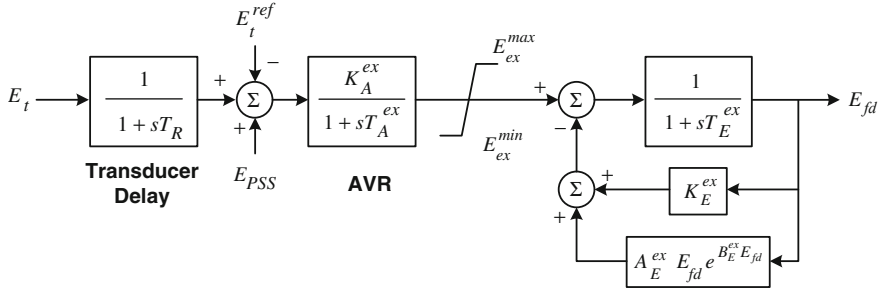


Fig. 2.3 Simplified block diagram for the IEEE Type DC1A DC exciter

Two versions of this controller are used within this thesis, referred to as ST1A_v1 and ST1A_v2.

- **ST1A_v1** treats the transducer delay as negligible ($T_R = 0$).
- **ST1A_v2** has no time constant in the exciter block ($T_A^{\text{ex}} = 0$), and no transient gain reduction block ($T_B^{\text{TGR}} = T_C^{\text{TGR}} = 0$).

2.1.2.3 DC Excitation (IEEE Type DC1A)

Excitation systems which use a DC current generator and commutator are referred to as DC exciters and typically respond more slowly than static systems [4]. Figure 2.3 presents a simplified version of the IEEE Type DC1A DC excitation system used within this thesis.

2.1.3 Power System Stabilisers

A power system stabiliser will act to add damping to generator rotor oscillations through a supplementary control signal sent to the excitation system. The most common [3] and logical signal to use to monitor generator rotor oscillations is the rotor speed deviation $\Delta\omega_r$ and this is used within this thesis.

Due to the phase characteristics of the excitation system through which the stabilising signal E_{PSS} must act, the PSS must include suitable phase compensation blocks to ensure the introduced electrical damping torque component is in phase with the rotor speed variation. This phase compensation is created by a number of phase lead/lag blocks which are combined with a washout filter so that steady state changes are ignored, and a gain K_{PSS} in order to maximise damping. The PSS block diagram is shown in Fig. 2.4. Limits on the supplementary control signal E_{PSS} are sometimes asymmetric to allow a large positive contribution during large swings, but limiting the negative output to reduce the risk of an under-voltage unit trip if the stabiliser fails [5]. The inclusion of a low-pass filter may be required to

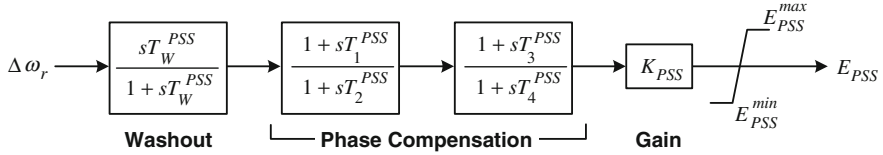


Fig. 2.4 Block diagram of a PSS

reduce the high-frequency output of the PSS in order to avoid potential interactions with the torsional mechanical modes of large steam-turbines—which can be as low as 7–8 Hz [3]. As these mechanical systems are not modelled within this work, there is no requirement to include the low-pass filter.

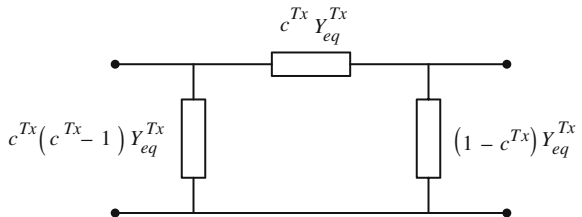
2.1.4 Transmission Lines

Throughout the work presented within this thesis, transmission lines are modelled using a lumped parameter model and the common π -representation [3]. The lines are assumed to be short enough that this approach is applicable and that more complex π -section or distributed parameter representation is not required [6].

2.1.5 Transformers

With orthogonal phase representation of the power system, an equivalent π -representation of a two-winding transformer can be used, as shown in Fig. 2.5 [3]. In this representation, $Y_{eq}^{Tx} = 1/Z_{eq}^{Tx}$ where Z_{eq}^{Tx} is the equivalent leakage reactance of the transformer, and $c^{Tx} = 1/\text{ONR}$ where ONR is the Off-Nominal turns Ratio of the transformer.

Fig. 2.5 Equivalent π -representation of a two winding transformer



2.1.6 Loads

The way in which power system loads are modelled can have a significant effect on the results obtained from simulations [7]. Electromechanical oscillations can affect voltage magnitude and frequency across the network and loads which are sensitive to these changes may require more detailed models to ensure accurate results. Further examples of the effects of load modelling can be found in [8]. Within this thesis, a constant impedance load model is used, represented as a shunt admittance Y_i^{load} connected to the i th load bus as in (2.16). This model is considered adequate for stability studies [1], although further studies involving more complex load models could be used in order to more accurately establish the system dynamic response. The modelling of system loads is not critical for the methodologies developed within this research and the use of a constant impedance representation is fully adequate for all the studies which have been performed.

$$Y_i^{load} = \frac{P_i^{load} - jQ_i^{load}}{V_i} \quad (2.16)$$

2.1.7 Network

The power system network is modelled simply as a combination of all transmission lines, transformers, and constant impedance loads. The nodal network equation formed, shown in (2.17) for a network with N buses, describes the relationship between system voltages \mathbf{V} and points of current injection \mathbf{I} [1].

$$\begin{bmatrix} I_1 \\ \vdots \\ I_i \\ \vdots \\ I_N \end{bmatrix} = \begin{bmatrix} Y_{11} & \dots & Y_{1i} & \dots & Y_{1N} \\ \vdots & \ddots & \vdots & \ddots & \vdots \\ Y_{i1} & \dots & Y_{ii} & \dots & Y_{iN} \\ \vdots & & \vdots & \ddots & \vdots \\ Y_{N1} & \dots & Y_{Ni} & \dots & Y_{NN} \end{bmatrix} \begin{bmatrix} V_1 \\ \vdots \\ V_i \\ \vdots \\ V_N \end{bmatrix} \text{ or } \mathbf{I} = \mathbf{YV} \quad (2.17)$$

In (2.17), subscripts i and j are bus numbers such that Y_{ii} is the self-admittance of bus i , and Y_{ij} is the mutual-admittance between buses i and j .

Reduction of the network model is possible so that all zero-injection buses are neglected and the *nodal network equation* has much smaller dimension [6]. This lowers the computational burden during simulations and power system analysis.

2.1.7.1 Network Reference Frames

The network is modelled in the common system reference frame (D - Q), however each machine is modelled using its own individual machine reference frame (d - q). Both of these orthogonal reference frames are rotating; the system reference frame at synchronous speed ω_{syn} , and each machine reference frame with the generator rotor, at ω_r , offset by the rotor angle δ . Transformations between reference frames for voltages are completed using (2.18) and (2.19), with transformations applied similarly for system current injections.

$$\begin{bmatrix} V_D \\ V_Q \end{bmatrix} = \begin{bmatrix} \sin \delta & \cos \delta \\ -\cos \delta & \sin \delta \end{bmatrix} \begin{bmatrix} V_d \\ V_q \end{bmatrix} \quad (2.18)$$

$$\begin{bmatrix} V_d \\ V_q \end{bmatrix} = \begin{bmatrix} \sin \delta & -\cos \delta \\ \cos \delta & \sin \delta \end{bmatrix} \begin{bmatrix} V_D \\ V_Q \end{bmatrix} \quad (2.19)$$

2.1.7.2 Network Disturbances

With a single phase representation of the network, only balanced faults can be simulated when assessing the non-linear transient response of the network. These are readily simulated by adding a large shunt admittance (a value of 10^9 pu is used within this thesis) to the *self-admittance* Y_{ii} of the faulted bus i in the *nodal admittance matrix*.

2.1.8 Modelling of Signal Time Delays

As wide area signals are often used as controller inputs for oscillation damping, the time delays associated with their transmission must be considered. The standard Laplace domain representation of the time-based function $f(t-\tau)$ subject to the signal transmission delay τ is given as $F(s) = e^{-\tau s}$. This must be approximated by a rational function for inclusion within a linearised power system model.

Padé approximations of time delays are commonly used with WAMS-based damping controllers where they have been shown to provide good results [9–12]. Within this thesis a second order approximation $P_2(s)$ is used, given by (2.20) [13].

$$P_2(s) = \frac{\tau^2 s^2 - 6\tau s + 12}{\tau^2 s^2 + 6\tau s + 12} \quad (2.20)$$

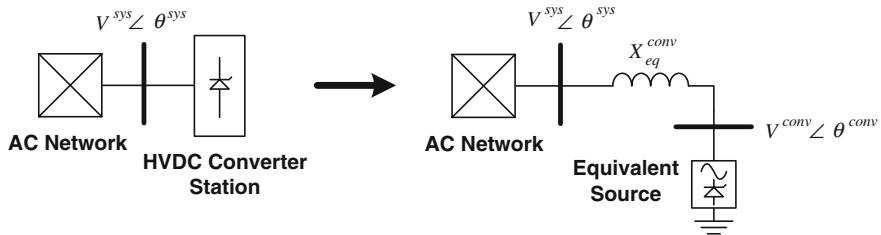


Fig. 2.6 Injection model for one HVDC converter station connected to an AC network

2.2 Modelling HVDC Systems

The technique used within this work to model HVDC systems for stability studies is injection modelling [14–17]. It is a flexible approach which can be used to model both LCC-HVDC and VSC-HVDC with varying levels of detail.

2.2.1 HVDC Converters

An HVDC converter station is modelled as a voltage source with variable magnitude V^{conv} and angle θ^{conv} connected to an AC bus across a reactance X_{eq}^{conv} , as shown in Fig. 2.6. Practically, this reactance represents the equivalent reactance between the converter station terminals and the point of common coupling with the AC system and is dominated by the leakage reactance of the converter transformer. By varying V^{conv} and θ^{conv} it is possible to produce the desired flow of active and reactive power from the DC system to the AC network or vice versa.

When an HVDC line is connected in parallel with an existing AC transmission line, the equivalent representation is therefore given by Fig. 2.7. The line shown

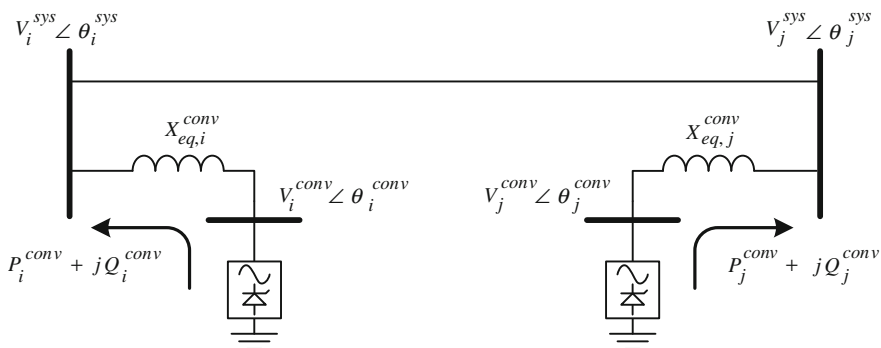


Fig. 2.7 Injection model for an HVDC transmission system in parallel with an existing AC line

between buses i and j represents the pre-existing AC line. The voltage and angle at the equivalent source buses can be varied to produce the desired converter power injection into the AC network. The injections of active and reactive power are dictated by (2.21) and (2.22) respectively.

$$P^{conv} = \frac{V^{conv} V^{sys} \sin(\theta^{conv} - \theta^{sys})}{X_{eq}^{conv}} \quad (2.21)$$

$$Q^{conv} = \frac{V^{conv} [V^{conv} - V^{sys} \cos(\theta^{conv} - \theta^{sys})]}{X_{eq}^{conv}} \quad (2.22)$$

Converter controls and DC line dynamics can be modelled to varying degrees of complexity, and the model can be extended for use with multi-terminal HVDC systems. This injection model can be easily integrated with existing AC network models as the interface point is the equivalent source bus voltage.

2.2.2 LCC-HVDC Modelling

LCC-HVDC systems cannot provide independent control of active and reactive power. They are controlled through variation of the converter firing angle α . From this single controllable parameter, the HVDC converter voltage can be calculated at the rectifier and inverter stations as in (2.33) and (2.24) respectively—assuming a generalised six-pulse converter [18].

$$V_{dc}^{rect} = \frac{3\sqrt{2}}{\pi} n V^{sys} \cos \alpha - \frac{3X_c}{\pi} I_{dc}^{rect} \quad (2.23)$$

$$V_{dc}^{inv} = \frac{3\sqrt{2}}{\pi} n V^{sys} \cos \beta + \frac{3X_c}{\pi} I_{dc}^{inv} \quad (2.24)$$

In (2.33) and (2.24), $\beta = 180^\circ - \alpha$, n is the converter transformer ratio, V^{sys} is the AC system voltage at the bus connected to the HVDC system, and X_c is the commutating reactance.

2.2.2.1 LCC-HVDC Converter Controls

Control of α is provided by Proportional-Integral (PI) controllers with clamped anti-windup as shown in Fig. 2.8. The rectifier controller maintains constant current with the current reference subjected to a standard Voltage Dependent Current Order Limiter (VDCOL) [3]. At the inverter the primary control aim is to maintain the DC system voltage. However current support is provided for situations when the DC current drops below a threshold equal to $I_{dc}^{ref} - I_{marg}$ (where I_{marg} is the current margin). Furthermore, at the inverter there is an added

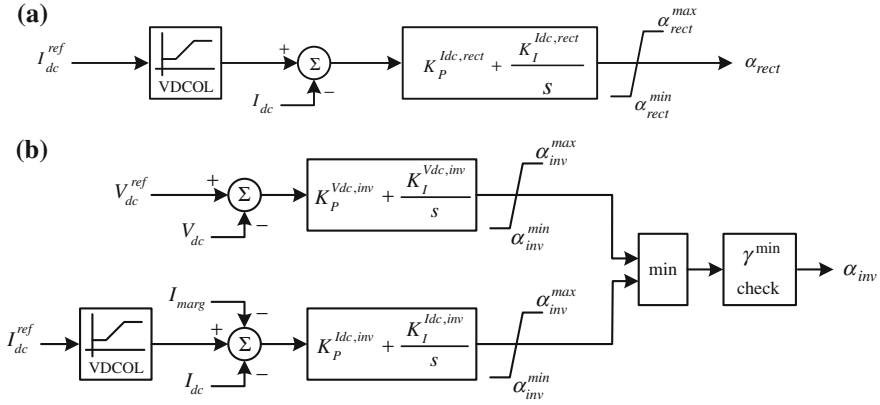


Fig. 2.8 LCC-HVDC injection model controller for **a** rectifier converter station, and **b** inverter converter station

constraint on α in that it cannot be set such that the extinction angle γ as calculated in (2.25) falls below γ^{min} (required to ensure full extinction of valves and avoid commutation failures) [18].

$$\gamma = \cos^{-1} \left[\left(V_{dc}^{inv} + \frac{3X_c}{\pi} I_{dc}^{inv} \right) / \frac{3\sqrt{2}}{\pi} n V^{sys} \right] \quad (2.25)$$

2.2.2.2 LCC-HVDC Line Modelling

For LCC-HVDC systems, a T -model is used to represent the DC system dynamics. Figure 2.9 illustrates this model, with the DC capacitance voltage and line currents described mathematically by (2.26–2.28) where C_{dc} , L_{dc} and R_{dc} are representative of the capacitance, inductance and resistance of the HVDC line [3]. This allows for simple calculation of the instantaneous power flow from the HVDC line to each converter station as (2.29). The convention that power flow from the DC system to the AC system is considered positive is maintained throughout this work.

$$\frac{d}{dt} I_{dc}^{rect} = \frac{1}{L_{dc}} (V_C - V_{dc}^{rect} - R_{dc} I_{dc}^{rect}) \quad (2.26)$$

$$\frac{d}{dt} I_{dc}^{inv} = \frac{1}{L_{dc}} (V_C - V_{dc}^{inv} - R_{dc} I_{dc}^{inv}) \quad (2.27)$$

$$\frac{d}{dt} V_C = \frac{1}{C_{dc}} (-I_{dc}^{rect} - I_{dc}^{inv}) \quad (2.28)$$

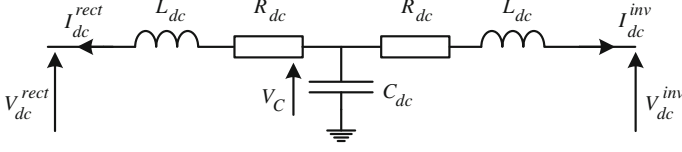


Fig. 2.9 LCC-HVDC line model

$$P_{dc} = I_{dc} V_{dc} \quad (2.29)$$

All symbols used in (2.26–2.29) are in accordance with Fig. 2.9. If converter stations are considered to be lossless then $P^{conv} = P_{dc}$, otherwise losses must be accounted for when calculating P^{conv} .

2.2.2.3 Reactive Power Compensation

The reactive power consumed by the LCC-HVDC converter is then given by (2.30), assuming reactive compensation is provided by a shunt susceptance B_{comp} [3].

$$Q^{conv} = -P^{conv} \tan \varphi + B_{comp} (V^{sys})^2 \quad (2.30)$$

In (2.30), φ is given by (2.31) at the rectifier and by (2.32) at the inverter.

$$\varphi^{rect} = \cos^{-1} \left(\cos \alpha - \frac{X_C I_{dc}^{rect}}{\sqrt{2} n V^{sys}} \right) \quad (2.31)$$

$$\varphi^{inv} = \cos^{-1} \left(\cos \beta + \frac{X_C I_{dc}^{inv}}{\sqrt{2} n V^{sys}} \right) \quad (2.32)$$

The active and reactive power injections to the AC network (P^{conv} and Q^{conv}) for an LCC-HVDC line are fully defined.

2.2.3 VSC-HVDC Modelling

VSC-HVDC is capable of providing four-quadrant power control consisting of any combination of positive or negative active and reactive power [19]. This is achieved through control of the converter bus voltage magnitude and angle. For point-to-point transmission systems a common and realistic control solution is used with one converter station maintaining DC voltage and the other regulating active power flow. Reactive power control is independent at each converter station [19].

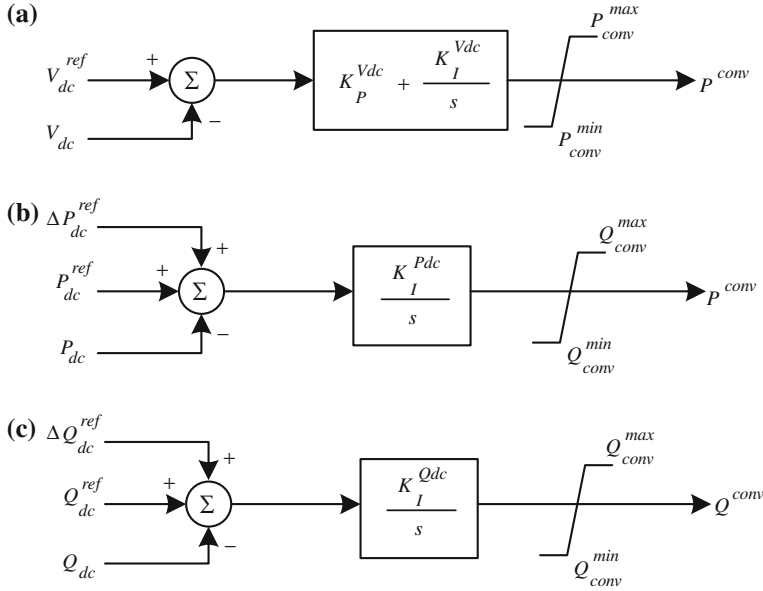


Fig. 2.10 VSC-HVDC injection model controller for **a** DC voltage, **b** active power, and **c** reactive power

2.2.3.1 VSC-HVDC Converter Controls

Controllers are PI or integral regulators with clamped anti-windup as shown in Fig. 2.10 [20]. Signals ΔP_{dc}^{ref} and ΔQ_{dc}^{ref} are to be used for auxiliary stabilising control action [15, 21].

2.2.3.2 VSC-HVDC Line Modelling

VSC-HVDC line dynamics are represented by a simple π -model within this research, as in Fig. 2.11. The DC line voltages and current are described mathematically by (2.33–2.35). As with the LCC-HVDC model, power flow from the DC system to the AC system is considered positive.

$$\frac{d}{dt} V_{dc,i} = \frac{1}{C_{dc}} \left(-\frac{P_{dc,i}}{V_{dc,i}} - I_{dc} \right) \quad (2.33)$$

$$\frac{d}{dt} V_{dc,j} = \frac{1}{C_{dc}} \left(-\frac{P_{dc,j}}{V_{dc,j}} + I_{dc} \right) \quad (2.34)$$

$$\frac{d}{dt} I_{dc} = \frac{1}{L_{dc}} (-I_{dc} R_{dc} + V_{dc,i} - V_{dc,j}) \quad (2.35)$$

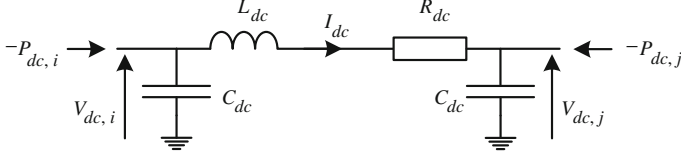


Fig. 2.11 VSC-HVDC line model based on power injection

All symbols used in (2.33–2.35) are in accordance with Fig. 2.11. As with LCC-HVDC lines, if converter stations are considered to be lossless then $P^{conv} = P_{dc}$.

2.2.4 Interface with AC System

As electromechanical oscillations with a typical frequency in the range of 0.2–2.5 Hz are being investigated within this research, the fast time constants associated with the switching operations of the power electronics can be neglected [15, 21]. It is therefore assumed that the converters are able to instantaneously reach the controller set-points P^{conv} and Q^{conv} in Fig. 2.10. Interface with the AC system requires setting the equivalent source voltage to ensure that these powers are injected into the AC network using (2.36) and (2.37).

$$V^{conv} = \sqrt{a^2 + b^2} \quad (2.36)$$

$$\theta^{conv} = \theta^{sys} + \tan^{-1}(a/b) \quad (2.37)$$

In (2.36) and (2.37), $a = V^{conv} \sin(\theta^{conv} - \theta^{sys})$ and $b = V^{conv} \cos(\theta^{conv} - \theta^{sys})$ are calculated using (2.38) and (2.39).

$$a = \frac{X_{eq}^{conv} P^{conv}}{V^{sys}} \quad (2.38)$$

$$b = \frac{1}{2} \left[V^{sys} + \sqrt{(V^{sys})^2 - 4 \left(\frac{(X_{eq}^{conv} P^{conv})^2}{(V^{sys})^2} - X_{eq}^{conv} Q^{conv} \right)} \right] \quad (2.39)$$

2.2.5 Multi-Terminal HVDC Grid Modelling

Extension of the point-to-point VSC-HVDC injection model to a multi-terminal grid is easily performed. The converter controls and interface equations remain the

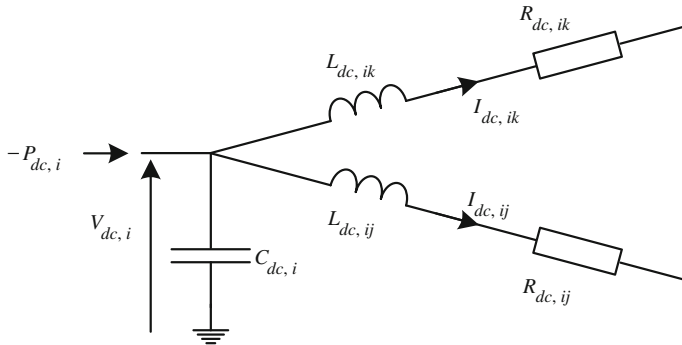


Fig. 2.12 Generic MTDC converter node line model

same. However the DC line equations require modification in order to represent a network, rather than a single line. As described fully in [16], the DC capacitance is lumped at the converter station terminals, and the lines are represented as purely resistive and inductive.

Using the generic MTDC converter node shown in Fig. 2.12, converter node Eqs. (2.40) and (2.41) can be used to describe the DC voltages and currents within the grid. The convention that power flow is positive when injected into the AC system from the DC system is still maintained. For the purposes of the local converter node equations, it is also assumed that all outgoing current flows from the node are positive.

$$\frac{d}{dt} V_{dc,i} = \frac{1}{C_{dc,i}} \left(-\frac{P_{dc,i}}{V_{dc,i}} - \sum_{j \neq i}^{n_{conv,i}} I_{dc,ij} \right) \quad (2.40)$$

$$\frac{d}{dt} I_{dc,ij} = \frac{1}{L_{dc,ij}} (-I_{dc,ij} R_{dc,ij} + V_{dc,i} - V_{dc,j}) \quad (2.41)$$

In (2.40) and (2.41), $n_{conv,i}$ is the number of converters connected to the i th converter through DC lines, and the subscript ij refers to the line connecting the i th and j th converters.

Within this thesis a simple extension of the point-to-point control schemes is used. One converter station within the MTDC grid will maintain the DC voltage—referred to as the slack DC bus. The remaining converter stations regulate active power flow with reactive power flow independently controlled at all converter stations. The controls presented previously in Fig. 2.10 are used. Use of more complex DC voltage droop characteristics are only of importance when studying the effects of transient events and outages, such as the loss of a converter station [22]. As these transient studies are not investigated as part of this research, the use of a slack DC bus is a suitable simplification.

2.2.6 HVDC Model Summaries

The equations which constitute the complete HVDC models are repeated for completeness in the following summary sections.

2.2.6.1 LCC-HVDC

A complete LCC-HVDC line is modelled as follows. The rectifier converter station is modelled using (2.42) with control from Fig. 2.8a.

$$V_{dc}^{rect} = \frac{3\sqrt{2}}{\pi} n V^{sys} \cos \alpha - \frac{3X_C}{\pi} I_{dc}^{rect} \quad (2.42)$$

The inverter converter station is modelled using (2.43–2.44) with control from Fig. 2.8b.

$$V_{dc}^{inv} = \frac{3\sqrt{2}}{\pi} n V^{sys} \cos \beta + \frac{3X_C}{\pi} I_{dc}^{inv} \quad (2.43)$$

$$\gamma = \cos^{-1} \left[\left(V_{dc}^{inv} + \frac{3X_C}{\pi} I_{dc}^{inv} \right) / \frac{3\sqrt{2}}{\pi} n V^{sys} \right] \quad (2.44)$$

The LCC-HVDC line currents and respective power flows are found using (2.45–2.48).

$$\frac{d}{dt} I_{dc}^{rect} = \frac{1}{L_{dc}} (V_C - V_{dc}^{rect} - R_{dc} I_{dc}^{rect}) \quad (2.45)$$

$$\frac{d}{dt} I_{dc}^{inv} = \frac{1}{L_{dc}} (V_C - V_{dc}^{inv} - R_{dc} I_{dc}^{inv}) \quad (2.46)$$

$$\frac{d}{dt} V_C = \frac{1}{C_{dc}} (-I_{dc}^{rect} - I_{dc}^{inv}) \quad (2.47)$$

$$P_{dc} = I_{dc} V_{dc} \quad (2.48)$$

P^{conv} is determined from P_{dc} considering the losses of the converter stations, with reactive power consumption calculated using (2.49) and (2.50) at the rectifier, and (2.49) and (2.51) at the inverter.

$$Q^{conv} = -P^{conv} \tan \varphi + B_{comp} (V^{sys})^2 \quad (2.49)$$

$$\varphi^{rect} = \cos^{-1} \left(\cos \alpha - \frac{X_C I_{dc}^{rect}}{\sqrt{2} n V^{sys}} \right) \quad (2.50)$$

$$\varphi^{inv} = \cos^{-1} \left(\cos \beta + \frac{X_C I_{dc}^{inv}}{\sqrt{2} n V_{sys}} \right) \quad (2.51)$$

Finally, the equivalent source voltages to ensure the correct injections of P^{conv} and Q^{conv} at each converter station are calculated using (2.52–2.73).

$$V^{conv} = \sqrt{a^2 + b^2} \quad (2.52)$$

$$\theta^{conv} = \theta^{sys} + \tan^{-1}(a/b) \quad (2.53)$$

$$a = \frac{X_{eq}^{conv} P^{conv}}{V_{sys}} \quad (2.54)$$

$$b = \frac{1}{2} \left[V^{sys} + \sqrt{(V^{sys})^2 - 4 \left(\frac{(X_{eq}^{conv} P^{conv})^2}{(V^{sys})^2} - X_{eq}^{conv} Q^{conv} \right)} \right] \quad (2.55)$$

2.2.6.2 VSC-HVDC

The model requirements for a point-to-point VSC-HVDC line are presented within this section. One converter operates with control schemes (a) and (c) from Fig. 2.10, and the other with control schemes (b) and (c) from Fig. 2.10. The VSC-HVDC system currents and voltages are determined by the line model which is defined using (2.56–2.58).

$$\frac{d}{dt} V_{dc,i} = \frac{1}{C_{dc}} \left(-\frac{P_{dc,i}}{V_{dc,i}} - I_{dc} \right) \quad (2.56)$$

$$\frac{d}{dt} V_{dc,j} = \frac{1}{C_{dc}} \left(-\frac{P_{dc,j}}{V_{dc,j}} + I_{dc} \right) \quad (2.57)$$

$$\frac{d}{dt} I_{dc} = \frac{1}{L_{dc}} (-I_{dc} R_{dc} + V_{dc,i} - V_{dc,j}) \quad (2.58)$$

The converters are assumed to reach the power injection controller set-points instantaneously [15, 21]. Therefore as with the LCC-HVDC line, the equivalent source voltages to ensure the correct injections of P^{conv} and Q^{conv} at each converter station are calculated using (2.59–2.62).

$$V^{conv} = \sqrt{a^2 + b^2} \quad (2.59)$$

$$\theta^{conv} = \theta^{sys} + \tan^{-1}(a/b) \quad (2.60)$$

$$a = \frac{X_{eq}^{conv} P^{conv}}{V^{sys}} \quad (2.61)$$

$$b = \frac{1}{2} \left[V^{sys} + \sqrt{(V^{sys})^2 - 4 \left(\frac{(X_{eq}^{conv} P^{conv})^2}{(V^{sys})^2} - X_{eq}^{conv} Q^{conv} \right)} \right] \quad (2.62)$$

2.2.6.3 VSC-MTDC

A VSC-MTDC system is modelled as an extension of a point-to-point VSC-HVDC line. One *slack* converter station uses control schemes (a) and (c) from Fig. 2.10 (to regulate voltage and reactive power). All other converter stations use control schemes (b) and (c) from Fig. 2.10. An example is presented the VSC-MTDC grid shown in Fig. 2.13, for which the mathematical model has been explicitly stated.

For clarity, C_{dc} , L_{dc} and R_{dc} have not been included in the diagram. At each converter station i there exists a capacitance $C_{dc,i}$. Each line between the i th and j th converter stations consists of a resistance $R_{dc,ij}$ and an inductance $L_{dc,ij}$.

The voltages at converter stations 1–4 are defined by (2.63–2.66), with all line currents calculated using (2.67–2.69) considering the identities (2.70–2.72).

$$\frac{d}{dt} V_{dc,1} = \frac{1}{C_{dc,1}} \left(-\frac{P_{dc,1}}{V_{dc,1}} - I_{dc,1-2} \right) \quad (2.63)$$

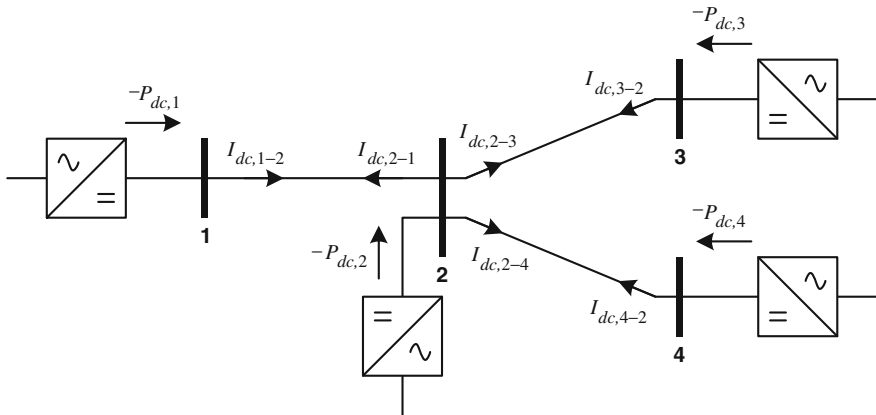


Fig. 2.13 Example of a four-node VSC-MTDC grid

$$\frac{d}{dt}V_{dc,2} = \frac{1}{C_{dc,2}} \left(-\frac{P_{dc,2}}{V_{dc,2}} - I_{dc,2-1} - I_{dc,2-3} - I_{dc,2-4} \right) \quad (2.64)$$

$$\frac{d}{dt}V_{dc,3} = \frac{1}{C_{dc,3}} \left(-\frac{P_{dc,3}}{V_{dc,3}} - I_{dc,3-2} \right) \quad (2.65)$$

$$\frac{d}{dt}V_{dc,4} = \frac{1}{C_{dc,4}} \left(-\frac{P_{dc,4}}{V_{dc,4}} - I_{dc,4-2} \right) \quad (2.66)$$

$$\frac{d}{dt}I_{dc,1-2} = \frac{1}{L_{dc,1-2}} (-I_{dc,1-2}R_{dc,1-2} + V_{dc,1} - V_{dc,2}) \quad (2.67)$$

$$\frac{d}{dt}I_{dc,2-3} = \frac{1}{L_{dc,2-3}} (-I_{dc,2-3}R_{dc,2-3} + V_{dc,2} - V_{dc,3}) \quad (2.68)$$

$$\frac{d}{dt}I_{dc,2-4} = \frac{1}{L_{dc,2-4}} (-I_{dc,2-4}R_{dc,2-4} + V_{dc,2} - V_{dc,4}) \quad (2.69)$$

$$I_{dc,1-2} = -I_{dc,2-1} \quad (2.70)$$

$$I_{dc,2-3} = -I_{dc,3-2} \quad (2.71)$$

$$I_{dc,2-4} = -I_{dc,4-2} \quad (2.72)$$

2.3 Power System Analysis Techniques

The various AC and DC components that make up the complete non-linear power system model have been described according to their differential and algebraic equations. This section will describe the further tools which are often used to assess power system small-disturbance stability and which facilitate the design of power system oscillation damping controllers.

2.3.1 Power System Linearisation

As described in [Chap. 1](#), small-disturbance stability is the ability of a power system to maintain synchronous operation when subjected to small disturbances [\[3\]](#). A disturbance is considered to be small if the power system equations can be linearised for the purpose of the analysis.

The power system is described by the compact vector–matrix representation of [\(2.73\)](#) and [\(2.74\)](#).

$$\dot{\mathbf{x}} = \mathbf{f}(\mathbf{x}, \mathbf{u}) \quad (2.73)$$

$$\mathbf{y} = \mathbf{g}(\mathbf{x}, \mathbf{u}) \quad (2.74)$$

In (2.73) and (2.74), \mathbf{x} is a vector of n state variables, \mathbf{u} is a vector of m system inputs, \mathbf{y} is a vector of p system outputs, and \mathbf{f} and \mathbf{g} are vectors of non-linear equations.

An equilibrium point can be defined at which $\mathbf{x} = \mathbf{x}_0$ and $\mathbf{u} = \mathbf{u}_0$ such that (2.73) is equal to zero. By making a small perturbation (Δ) from this point, (2.75) can be established.

$$\dot{\mathbf{x}}_0 + \Delta \dot{\mathbf{x}} = \mathbf{f}(\mathbf{x}_0 + \Delta \mathbf{x}, \mathbf{u}_0 + \Delta \mathbf{u}) \quad (2.75)$$

As only small perturbations are considered, a first order Taylor's series expansion of (2.75) can be used as a suitable approximation [3]. This can be similarly completed for (2.74) with respect to system outputs, and simplified, to provide the linearised *state space* power system model consisting of (2.76) and (2.77).

$$\Delta \dot{\mathbf{x}} = \mathbf{A} \Delta \mathbf{x} + \mathbf{B} \Delta \mathbf{u} \quad (2.76)$$

$$\Delta \mathbf{y} = \mathbf{C} \Delta \mathbf{x} + \mathbf{D} \Delta \mathbf{u} \quad (2.77)$$

In (2.76) and (2.77), the following definitions are used:

$$\mathbf{A} = \begin{bmatrix} \frac{\partial f_1}{\partial x_1} & \cdots & \frac{\partial f_1}{\partial x_n} \\ \vdots & \ddots & \vdots \\ \frac{\partial f_n}{\partial x_1} & \cdots & \frac{\partial f_n}{\partial x_n} \end{bmatrix}, \mathbf{B} = \begin{bmatrix} \frac{\partial f_1}{\partial u_1} & \cdots & \frac{\partial f_1}{\partial u_m} \\ \vdots & \ddots & \vdots \\ \frac{\partial f_n}{\partial u_1} & \cdots & \frac{\partial f_n}{\partial u_m} \end{bmatrix},$$

$$\mathbf{C} = \begin{bmatrix} \frac{\partial g_1}{\partial x_1} & \cdots & \frac{\partial g_1}{\partial x_n} \\ \vdots & \ddots & \vdots \\ \frac{\partial g_p}{\partial x_1} & \cdots & \frac{\partial g_p}{\partial x_n} \end{bmatrix}, \mathbf{D} = \begin{bmatrix} \frac{\partial g_1}{\partial u_1} & \cdots & \frac{\partial g_1}{\partial u_m} \\ \vdots & \ddots & \vdots \\ \frac{\partial g_p}{\partial u_1} & \cdots & \frac{\partial g_p}{\partial u_m} \end{bmatrix}$$

2.3.2 Modal Analysis

By Lyapunov's first method, the small-disturbance stability of a system is given by the roots of the characteristic equation of the system first order approximations [23]. With respect to the linearised state space model of the power system, calculation of the eigenvalues of the system matrix \mathbf{A} is required.

The eigenvalues of \mathbf{A} are given by the values of the scalar λ for which there are non-trivial solutions to (2.78), where ϕ is an $n \times 1$ vector and $\phi \neq 0$. There are n solutions to (2.78), forming the set of n eigenvalues (or modes) $\lambda = \lambda_1, \lambda_2, \dots, \lambda_n$.

$$\mathbf{A}\phi = \lambda\phi \quad (2.78)$$

The column vector ϕ_i which satisfies (2.78) for the i th eigenvalue λ_i is referred to as the *right eigenvector* of \mathbf{A} associated with λ_i . Similarly there exists a *left eigenvector*, a $1 \times n$ row vector ψ which satisfies (2.79) for λ_i .

$$\psi\mathbf{A} = \psi\lambda \quad (2.79)$$

As both right and left eigenvectors are unit-less, it is common practice to normalise them such that $\phi_i\psi_i = 1$.

The modal matrices are often used to succinctly express the eigenproperties of a system. These $n \times n$ matrices are defined by (2.80–2.82).

$$\Phi = [\phi_1 \phi_2 \dots \phi_n] \quad (2.80)$$

$$\Psi = [\psi_1 \psi_2 \dots \psi_n]^T \quad (2.81)$$

$$\Lambda = \text{diag}[\lambda_1 \lambda_2 \dots \lambda_n] \quad (2.82)$$

In (2.80–2.82), Φ is the matrix of right eigenvectors, Ψ is the matrix of left eigenvectors, and Λ is a diagonal matrix of system eigenvalues.

Within this thesis, the MATLAB/Simulink environment is used to provide linearised system models and perform eigenvalue analysis.

2.3.2.1 Modal Stability

The time-based behaviour of a mode λ_i is given by $e^{\lambda_i t}$ [1]. It can therefore be easily established that purely real eigenvalues are non-oscillatory. Negative real eigenvalues will result in a time response which decays, whereas positive real eigenvalues will lead to an aperiodically increasing time response. If \mathbf{A} is real, complex eigenvalues occur only in conjugate pairs ($\lambda = \sigma \pm j\omega$). These oscillatory modes are described by their *damping* σ and *frequency* ω . The *damping factor* ζ of a mode is defined as in (2.83) and provides the rate of decay of the amplitudes of oscillation associated with the mode. If a complex eigenvalue has positive real part, these oscillations will grow and lead to system instability.

$$\zeta = \frac{-\sigma}{\sqrt{\sigma^2 + \omega^2}} \quad (2.83)$$

It can be concluded that if any single eigenvalue has a positive real part, the system is unstable. Furthermore, in practical power system applications, it is desirable to restore steady state operation as quickly as possible following disturbances. High

damping factors for electromechanical modes are therefore desired, with a typical threshold of $\zeta > 5\%$ often implemented for control design purposes [24].

2.3.2.2 Modal System Representation

The state space power system model given by (2.76) and (2.77) can be rewritten in the modal canonical form of (2.84) and (2.85) by means of a modal transformation of the state variables $\Delta \mathbf{x}$ to the modal variables \mathbf{z} as in (2.86).

$$\dot{\mathbf{z}} = \mathbf{\Lambda} \mathbf{z} + \mathbf{B}_M \Delta \mathbf{u} \quad (2.84)$$

$$\Delta \mathbf{y} = \mathbf{C}_M \mathbf{z} + \mathbf{D} \Delta \mathbf{u} \quad (2.85)$$

$$\mathbf{z} = \mathbf{M} \Delta \mathbf{x} \quad (2.86)$$

In (2.84–2.86), the modal transformation matrix $\mathbf{M} = \mathbf{\Phi}^{-1}$, and the modal state matrices are defined as $\mathbf{\Lambda} = \mathbf{M} \mathbf{A} \mathbf{M}^{-1}$, $\mathbf{B}_M = \mathbf{M} \mathbf{B}$, and $\mathbf{C}_M = \mathbf{C} \mathbf{M}^{-1}$.

The $n \times m$ matrix \mathbf{B}_M is the *mode controllability matrix* and defines how controllable a mode is through a given input. If the element $\mathbf{B}_M(i, j)$ is equal to zero, then the j th input will have no effect on the i th mode [3].

The $p \times n$ matrix \mathbf{C}_M is the *modal observability matrix* which defines how observable a mode is in a given output. If the element $\mathbf{C}_M(k, i)$ is equal to zero, then the i th mode cannot be observed in the k th output [3].

Residue values contain information about both modal observability in a given output, and controllability through a given input. The open loop residue of the system transfer function between the j th input and k th output, with respect to the i th mode, is given by (2.87). The complex entries in \mathbf{R}_i also contain information about the phase delay between system inputs and outputs which is useful for control purposes [3].

$$\mathbf{R}_i(j, k) = \mathbf{C}_M(k, i) \mathbf{B}_M(i, j) \quad (2.87)$$

2.4 Damping Controller Design

It was shown in Chap. 1 that HVDC systems can be exploited for POD purposes. This section will briefly present the POD controller designs that have been used within this thesis. It should be noted that these are not the only POD controller methodologies available, and many alternative schemes have been discussed further in Sect. 1.3.1. The two controllers described below are the PSS structure, and modal linear quadratic Gaussian control. These two controller forms offer different advantages and vary significantly in complexity.

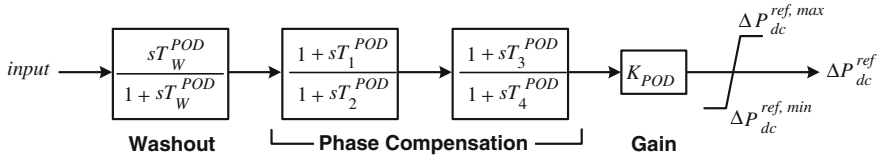


Fig. 2.14 PSS-based POD controller structure

2.4.1 PSS-Based POD Control

A simple supplementary POD controller design commonly used with HVDC systems follows the conventional structure of a PSS incorporating washout, phase compensation, gain, and limits as shown in Fig. 2.14. This design has been used numerous times in previous studies, for example [25–28]. The control structure is simple, effective, and easily tuned; it can however only be optimally tuned for a single mode.

Input to the controller is usually selected as a local input, although PSS designs incorporating wide area signals also exist [29–31]. Throughout this thesis, signal selection will be specified for each case study presented.

Controller parameters are specified using the residue-based tuning approach [32–34]. Once the controller output (ΔP_{dc}^{ref}) and the controller input are known, the open loop transfer function residues for each electromechanical mode requiring additional damping can be determined using (2.87). POD controller tuning is carried out for the mode with the greatest residue magnitude $|R_i|$ as it will be most affected by the controller [32, 33].

Having established the mode to be damped, the residue angle $\angle R_i$ is determined. The phase compensation required within the PSS-based POD controller is then calculated as $180^\circ - \angle R_i$. This will move the target eigenvalue further into the left half of the complex plane with no change in frequency [33, 34]. Parameters for the lead-lag blocks are determined according to the required phase compensation. Phase compensation is limited to approximately 60° per block to reduce sensitivity to noise at high frequencies as well as due to the physical limitations of RLC circuits [35, 36]. Following this, controller gain K_{POD} is increased until a sufficient amount of damping is achieved for the target mode, taking care to avoid causing detrimental effects to the other system eigenvalues and ensuring a suitable PSS gain margin [35, 36]. Final controller parameters will be presented for each case study throughout this thesis.

2.4.2 Modal Linear Quadratic Gaussian Control

A control approach capable of using multiple wide area signals to improve the damping of a number of targeted modes has also been studied. This controller structure can also be extended to a multiple-output configuration. This is necessary

when coordinated damping using more than one VSC-HVDC line or an MTDC grid is considered.

The linear quadratic Gaussian control design is a cornerstone of modern optimal control theory and its advantages have led to widespread research into its use in power system damping [10, 37–40]. However, the design approach is rarely straightforward, especially within large power systems where many generators participate in the critical modes which require additional damping. In these situations, the controller tuning process can become prohibitively complex.

Participation factor analysis is required in order to identify the electromechanical states involved in critical system modes [3]. Weightings can then be assigned to these states. However, if these states are involved in other targeted modes or modes that do not require altering, the damping of these modes will also be affected, sometimes adversely. This results in a complex and time consuming tuning process in which it is often not possible to obtain exact target damping factors. These complexities and problems can be overcome through the novel use of a modal representation of the control design problem. The formulation of this control structure and extensive studies are presented in [12]. A brief description is presented below.

The power system model is linearised to (2.88) and (2.89), where \mathbf{w} and \mathbf{v} are assumed to be uncorrelated zero-mean Gaussian stochastic noise processes with constant power spectral density matrices \mathbf{W} and \mathbf{V} respectively [41]. Note that \mathbf{D} from (2.85) is neglected as it is typically equal to zero for all power system applications.

$$\dot{\mathbf{x}} = \mathbf{A}\mathbf{x} + \mathbf{B}\mathbf{u} + \Gamma\mathbf{w} \quad (2.88)$$

$$\mathbf{y} = \mathbf{C}\mathbf{x} + \mathbf{v} \quad (2.89)$$

The standard LQG feedback control law can be written simply as (2.90).

$$\mathbf{u}(t) = -\mathbf{K}\hat{\mathbf{x}}(t) \quad (2.90)$$

The Linear Quadratic Regulator (LQR) gain \mathbf{K} is determined by solving the associated Algebraic Riccati Equation (ARE) to minimise the cost function (2.91). In this modal formulation, the real matrix \mathbf{M} is the modal transformation matrix described previously in Sect. 2.3.2.2, obtained using real Schur decomposition [42]. This transformation to the modal variables, as in (2.86), allows targeted damping on specific system modes through appropriate, commonly diagonal, setting of the weighting matrices \mathbf{Q}_M and \mathbf{R} .

$$\mathbf{J}_K = \lim_{T \rightarrow \infty} \mathbf{E} \left\{ \int_0^T (\mathbf{x}^T (\mathbf{M}^T \mathbf{Q}_M \mathbf{M}) \mathbf{x} + \mathbf{u}^T \mathbf{R} \mathbf{u}) dt \right\} \quad (2.91)$$

Values of \mathbf{R} are set in order to penalise the corresponding controller's outputs from high actions. Values of \mathbf{Q}_M are set in order to effect a higher effort by the controller to stabilise the corresponding modal variables \mathbf{z}_i , and hence $e^{\lambda_i t}$

Non-zero weights are given only to modes of interest in \mathbf{Q}_M , thus targeting the control effort of the LQR while keeping the locations of other modes unaltered.

With respect to (2.90) $\hat{\mathbf{x}}$ is an estimate of the states \mathbf{x} obtained using a Kalman filter as described by (2.92).

$$\dot{\hat{\mathbf{x}}}(t) = \mathbf{A}\hat{\mathbf{x}} + \mathbf{B}\mathbf{u} + \mathbf{L}(\mathbf{y} - \mathbf{C}\hat{\mathbf{x}}) + \mathbf{L}\mathbf{v} \quad (2.92)$$

The optimal choice of the constant estimation error feedback matrix \mathbf{L} minimises $\mathbf{E}\{[\mathbf{x} - \hat{\mathbf{x}}]^T[\mathbf{x} - \hat{\mathbf{x}}]\}$. It is calculated by solving the ARE associated with the cost function (2.93). The weighting matrices \mathbf{W} and \mathbf{V} are calculated as in (2.94) and (2.95) and tuned according to the Loop Transfer Recovery (LTR) procedure at plant input [41].

$$J_L = \lim_{T \rightarrow \infty} \mathbf{E} \left\{ \int_0^T (\mathbf{x}^T \mathbf{W} \mathbf{x} + \mathbf{u}^T \mathbf{V} \mathbf{u}) dt \right\} \quad (2.93)$$

$$\mathbf{W} = \mathbf{\Gamma} \mathbf{W}_o \mathbf{\Gamma}^T + q \mathbf{B} \mathbf{\Theta} \mathbf{B}^T \quad (2.94)$$

$$\mathbf{V} = \mathbf{V}_o \quad (2.95)$$

In (2.94) and (2.95), \mathbf{W}_o and \mathbf{V}_o are estimates of the nominal model noise, and $\mathbf{\Theta}$ is any positive definite matrix.

Full recovery of robustness is achieved as $q \rightarrow \infty$. Care should be taken though, as full recovery would lead to excessively high gains and the nominal performance of the controller with respect to the true noise problem would therefore deteriorate. For non-minimum phase systems, which is commonly the case in power systems, only partial recovery can be achieved [41].

The MLQG controller has the structure shown in Fig. 2.15. The closed-loop dynamics of the LQG controller are described by (2.96). The transfer function for the complete LQG controller from \mathbf{y} to \mathbf{u} is given by (2.97).

$$\frac{d}{dt} \begin{bmatrix} \mathbf{x} \\ \hat{\mathbf{x}} \end{bmatrix} = \begin{bmatrix} \mathbf{A} & -\mathbf{B}\mathbf{K} \\ \mathbf{L}\mathbf{C} & \mathbf{A} - \mathbf{L}\mathbf{C} - \mathbf{B}\mathbf{K} \end{bmatrix} \begin{bmatrix} \mathbf{x} \\ \hat{\mathbf{x}} \end{bmatrix} + \begin{bmatrix} \mathbf{\Gamma}\mathbf{w} \\ \mathbf{L}\mathbf{v} \end{bmatrix} \quad (2.96)$$

$$\mathbf{K}_{LQG}(s) = \begin{bmatrix} \mathbf{A}_C & \mathbf{B}_C \\ \mathbf{C}_C & \mathbf{D}_C \end{bmatrix} = \begin{bmatrix} \mathbf{A} - \mathbf{B}\mathbf{K} - \mathbf{L}\mathbf{C} & \mathbf{L} \\ -\mathbf{K} & 0 \end{bmatrix} \quad (2.97)$$

Input signal selection is very important in order to capture as much information as possible regarding the critical modes that require improved damping. The methods used for signal selection and details of any signal delays will be discussed when specific case studies are presented throughout the thesis.

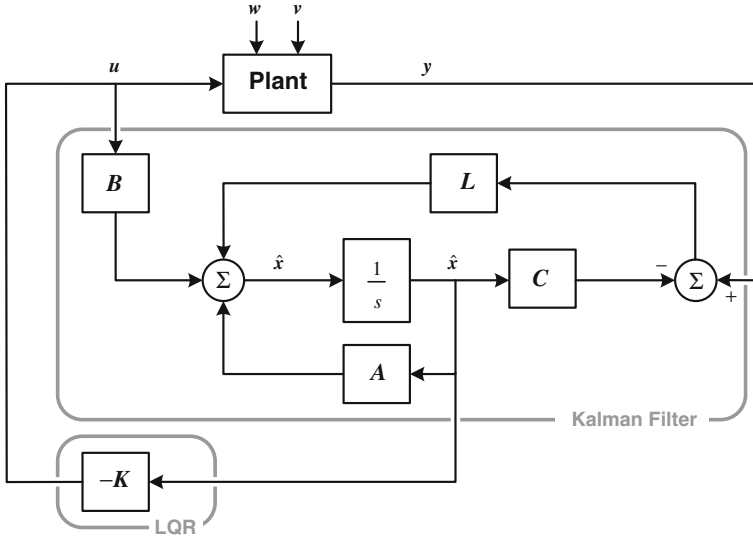


Fig. 2.15 Standard LQG controller structure

2.4.2.1 Model Reduction

As can be seen from (2.97), the final MLQG controller is of the same order as the plant model on which it is designed. It is often desirable to obtain a lower order controller in order to ensure that it is not too complex for practical implementation [41]. The possibility exists to reduce the order of the final controller at various stages of the design process. This reduction can occur:

- **On the plant model** prior to commencing the design procedure. When designing LQG controllers, it is sometimes necessary to perform initial model order reduction to avoid ill conditioning when solving high order matrix Riccati equations [39]. Following this reduction, signal delays are introduced where appropriate on inputs and outputs. The reduced plant model including delays is then used during the control design process.
- **On the final controller design** after completion of the design process. This will lessen the online computational burden of the controller whilst still maintaining the improved critical mode damping.
- **Both on the plant model and the final controller design** in order to minimise the final controller size.

Throughout this research, the *Schur Balanced Truncation Method* [43] has been used to perform model reduction – implemented within MATLAB. The rigorous comparison of the frequency response of the singular values of the full and reduced order systems is used to ensure that only system states having little effect on the *input–output* behaviour of the system are discarded [44].

In order to ensure clarity, the model reduction details for individual case studies within this thesis will be explicitly stated.

The research methods and results presented throughout this thesis are not dependent on the controller designs or tuning methods employed and further techniques, such as those previously discussed in [Sect. 1.3.1](#), could also be used.

2.5 Test Networks

Throughout this thesis two standard test networks are used. The standard AC networks are presented in the following sections. When HVDC modifications are made for the various studies conducted (such as the addition of point-to-point lines or an MTDC grid) they will be detailed on a case-by-case basis to avoid ambiguity.

All system details including line parameters, standard loading, and dynamic machine data is included in Appendix A. In all cases, initial load flows are performed using modified MATPOWER functions [\[45\]](#).

2.5.1 Two Area Network

A small four-machine, two-area network is introduced in [\[3\]](#) for use with small-disturbance stability studies. The network diagram is shown in [Fig. 2.16](#). This system requires significant transmission of power from bus 7 to bus 9 through a long transmission corridor, with the left and right areas of the network prone to post-disturbance inter-area oscillations. All generators are modelled as fifth order neglecting leakage reactance, and controlled by type ST1A_v1 static exciters with PSSs installed. All power system loads are modelled as constant impedance.

The power system exhibits three electromechanical oscillatory modes. At the nominal operating point given in Appendix A, these modes have the properties which are given in [Table 2.1](#).

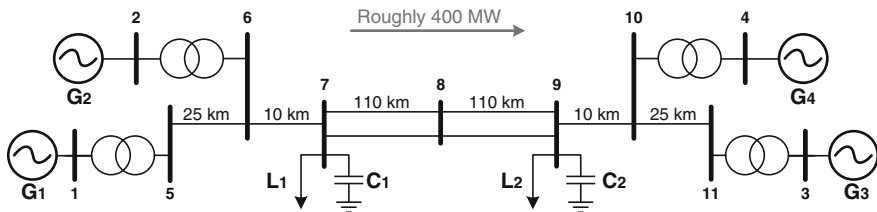


Fig. 2.16 Kundur two-area test network diagram

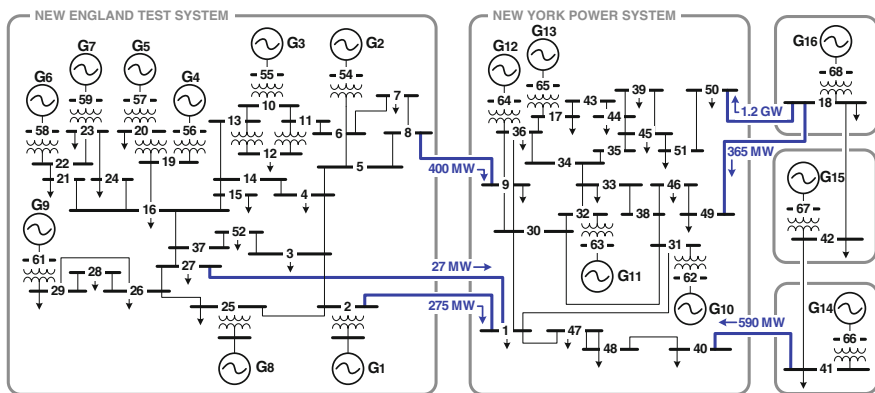
Table 2.1 Electromechanical mode properties for the two area test system at the nominal operating point

Mode	Description	Eigenvalue, $\lambda = \sigma + j\omega$ (pu)	Frequency, f (Hz)	Damping factor, ζ (%)
Mode 1	Local mode between G1 and G2	$-0.332 \pm j6.022$	0.958	5.50
Mode 2	Local mode between G3 and G4	$-0.349 \pm j6.232$	0.992	5.58
Mode 3	Inter-area mode between all generators	$-0.137 \pm j3.472$	0.553	3.94

2.5.2 New England Test System and New York Power System

A larger 16-machine, 68-bus, five-area network is also utilised throughout this thesis to investigate oscillatory behaviour. The network is shown in Fig. 2.17 and was introduced in [24] and used extensively in [44] for damping controller design studies. The network represents a reduced order equivalent model of the New England Test System (NETS) and the New York Power System (NYPS). Five separate areas are present: NETS consisting of G1-G9, NYPS consisting of G10-G13, and three further infeeds from neighbouring areas are represented separately by G14, G15 and G16. Flows of active power across inter-area ties are shown in Fig. 2.17, demonstrating the heavy import of power into the NYPS area, due to a generation shortfall of roughly 2.7 GW.

All generators are represented by full sixth order models. Generators G1-G8 use the slow DC1A exciter, whilst G9 is equipped with a fast acting ST1A_v2 static exciter and PSS. The remaining generators (G10-G16) are under constant manual excitation. Power system loads are modelled as constant impedance.

**Fig. 2.17** NETS-NYPS five-area test network diagram

The network exhibits four inter-area modes with a frequency of less than 1 Hz and poor damping factors of less than 5 %. The remaining eleven local modes have frequencies between 1–1.6 Hz and damping factors between 5.6–16.0 % and are all suitably damped.

2.6 Summary

This chapter has presented the fundamental modelling and analysis techniques which will be used throughout this thesis.

The chapter began by presenting the mathematical models of the components that form power systems. These included traditional AC apparatus including synchronous generators and their associated controls, transformers, transmission lines and loads, as well as describing the modelling of VSC-HVDC systems.

The way in which non-linear power system models can be linearised in order to conduct small-disturbance stability analysis was then discussed. The modal analysis techniques introduced then formed the basis of the linear POD controller designs. The two controller structures described in this chapter will be used throughout the thesis and their impact on system stability and performance in the presence of uncertainties will be assessed. Finally, the test networks used throughout this research have been introduced.

The following chapters will utilise these models, controller designs, and analysis techniques to perform a thorough investigation into the effects of HVDC on system stability.

References

1. J. Machowski, J.W. Bialek, J.R. Bumby, *Power System Dynamics and Stability* (John Wiley and Sons, Inc., Chichester, 1997)
2. P.W. Sauer, M.A. Pai, *Power System Dynamics and Stability* (Prentice Hall, Inc., Upper Saddle River, 1998)
3. P. Kundur, *Power System Stability and Control* (McGraw-Hill, Inc., London, 1994)
4. "IEEE Recommended Practice for Excitation System Models for Power System Stability Studies," *IEEE Std 421.5-2005* (Revision of IEEE Std **421**, 5-1992), 2006
5. E.V. Larsen, D.A. Swann, Applying power system stabilizers parts I, II and III. *IEEE Trans. Power Apparatus Syst.* **100**, 3017–3046 (1981)
6. P.M. Anderson, A.A. Fouad, *Power System Control and Stability*. (IEEE Press, New York, 1994)
7. IEEE Task Force on Load Representation for Dynamic Performance, "Load representation for dynamic performance analysis [of power systems]," *IEEE Trans on Power Systems*, **8**, pp. 472–482, 1993
8. C. Concordia, S. Ihara, Load representation in power system stability studies. *IEEE Trans. Power Apparatus Syst.* **101**, 969–977 (1982)
9. J.H. Chow, J.J. Sanchez-Gasca, R. Haoxing, W. Shaopeng, Power system damping controller design-using multiple input signals. *IEEE Control Syst. Mag.* **20**, 82–90 (2000)

10. D. Dotta, A.S. e Silva, I.C. Decker, Wide-area measurements-based two-level control design considering signal transmission delay. *IEEE Trans Power Syst.* **24**, 208–216 (2009)
11. T. Zabaoui, F. Okou, L.A. Dessaint, O. Akhrif, Time-delay compensation of a wide-area measurements-based hierarchical voltage and speed regulator. *Can. J. Electr. Comput. Eng.* **33**, 77–85 (2008)
12. A. Almutairi, *Enhancement of Power System Stability using Wide Area Measurement System Based Damping Controller* (Ph.D. School of Electrical and Electronic Engineering, University of Manchester, Manchester, 2010)
13. J. Lam, Model reduction of delay systems using Pade approximants. *Int. J. Control* **57**, 377–391 (1993)
14. S. Cole, R. Belmans, A proposal for standard VSC HVDC dynamic models in power system stability studies. *Electr. Power Syst. Res.* **81**, 967–973 (2011)
15. H.F. Latorre, M. Ghandhari, L. Söder, Active and reactive power control of a VSC-HVdc. *Electr. Power Syst. Res.* **78**, 1756–1763 (2008)
16. S. Cole, J. Beerten, R. Belmans, Generalized dynamic VSC MTDC model for power system stability studies. *IEEE Trans. Power Syst.* **25**, 1655–1662 (2010)
17. J. Arrillaga, N.R. Watson, *Computer Modelling of Electrical Power Systems*, 2nd edn. (Wiley, Chichester, 2001)
18. J. Arrillaga, *High Voltage Direct Current Transmission*, 2nd edn. (The Institute of Electrical Engineers, London, 1998)
19. J. Arrillaga, Y.H. Liu, N.R. Watson, *Flexible Power Transmission: The HVDC Options* (Wiley, Chichester, 2007)
20. C. Feltes, H. Wrede, F.W. Koch, I. Erlich, Enhanced fault ride-through method for wind farms connected to the grid through VSC-based HVDC transmission. *IEEE Trans. Power Syst.* **24**, 1537–1546 (2009)
21. P.E. Bjorklund, K. Srivastava, W. Quaintance, HvdC light modeling for dynamic performance analysis, in *Power Systems Conference and Exposition (PSCE)*, Atlanta, USA, 2006, pp. 871–876
22. J. Beerten, D.V. Hertem, R. Belmens, “VSC MTDC Systems with a Distributed Voltage Control—A Power Flow Approach,” presented at the *IEEE PowerTech* (Trondheim, Norway, 2011)
23. A.M. Lyapunov, *Stability of Motion (English Translation)* (Academic Press, Inc., London, 1967)
24. G. Rogers, *Power System Oscillations* (Kluwer Academic Publishers, Norwell, 2000)
25. C. Zheng, X. Zhou, L. Ruomei, Dynamic modeling and transient simulation for VSC based HVDC in multi-machine system, in *International Conference on Power System Technology (PowerCon)*, Chongqing, China, 2006, pp. 1–7
26. H. Jingbo, L. Chao, W. Xiaochen, W. Jingtao, T.S. Bi, Design and experiment of heuristic adaptive HVDC supplementary damping controller based on online Prony analysis, in *IEEE Power Engineering Society General Meeting*, 2007
27. Y. Pipelzadeh, B. Chaudhuri, T.C. Green, wide-area power oscillation damping control through HVDC: a case study on Australian equivalent system, in *IEEE Power and Energy Society General Meeting*, Minneapolis, USA, 2010
28. D.V. Hertem, R. Eriksson, L. Soder, M. Ghandhari, Coordination of multiple power flow controlling devices in transmission systems, in *IET ACDC*, London, UK, 2010
29. N. Yang, Q. Liu, J.D. McCalley, TCSC controller design for damping interarea oscillations. *IEEE Trans. Power Syst.* **13**, 1304–1310 (1998)
30. M.E. Aboul-El, A.A. Sallam, J.D. McCalley, A.A. Fouad, Damping controller design for power system oscillations using global signals. *IEEE Trans. Power Syst.* **11**, 767–773 (1996)
31. J. He, C. Lu, X. Wu, P. Li, J. Wu, Design and experiment of wide area HVDC supplementary damping controller considering time delay in China southern power grid. *IET Gener. Transm. Distrib.* **3**, 17–25 (2009)
32. J.V. Milanovic S.K. Yee, Roadmap for tuning power system controllers, in *IASTED Conference on Power and Energy Systems*, Marbella, Spain, 2003, pp. 763–770

33. F.L. Pagola, I.J. Perez-Arriaga, G.C. Verghese, On sensitivities, residues and participations. Applications to oscillatory stability analysis and control. *IEEE Power Eng. Rev.* **9**, 61–61 (1989)
34. L. Rouco, F.L. Pagola, An eigenvalue sensitivity approach to location and controller design of controllable series capacitors for damping power system oscillations. *IEEE Trans. Power Syst.* **12**, 1660–1666 (1997)
35. K. Ogata, *Modern Control Engineering*, 4th edn. (Prentice Hall, Minnesota, 2002)
36. N.S. Nise, *Control Systems Engineering*, 3rd edn. (Wiley, California, 2000)
37. T. Michigami, M. Terasaki, N. Sasazima, K. Hayashi, T. Okamoto, Development of a new adaptive LQG system generator for high-speed damping control techniques of power system oscillation. *Electr. Eng. Jpn.* **142**, 30–40 (2003)
38. A.C. Zolotas, B. Chaudhuri, I.M. Jaimoukha, P. Korba, A Study on LQG/LTR control for damping inter-area oscillations in power systems. *IEEE Trans. Control Syst. Technol.* **15**, 151–160 (2007)
39. K.M. Son, J.K. Park, On the robust LQG control of TCSC for damping power system oscillations. *IEEE Trans. Power Syst.* **15**, 1306–1312 (2000)
40. A.M.D. Ferreira, J.A.L. Barreiros, J.W. Barra, J.R. Brito-de-Souza, A robust adaptive LQG/LTR TCSC controller applied to damp power system oscillations. *Electr. Power Syst. Res.* **77**, 956–964 (2007)
41. S. Skogestad, I. Postlethwaite, *Multivariable Feedback Control: Analysis and Design* (Wiley, Chichester, 1996)
42. G.H. Golub, C.F.V. Loan, *Matrix Computations* (The John Hopkins University Press, Baltimore, 1989)
43. M.G. Safonov, R.Y. Chiang, A Schur method for balanced-truncation model reduction. *IEEE Trans. Autom. Control* **34**, 729–733 (1989)
44. B. Pal, B. Chaudhuri, *Robust Control in Power Systems* (Springer Inc., New York, 2005)
45. R.D. Zimmerman, C.E. Murillo-Sanchez, R.J. Thomas, MATPOWER: steady-state operations, planning, and analysis tools for power systems research and education. *IEEE Trans. Power Syst.* **26**, 12–19 (2011)

Improving the Stability of Meshed Power Networks
A Probabilistic Approach Using Embedded HVDC Lines

Preece, R.

2013, XXI, 188 p. 78 illus., 52 illus. in color., Hardcover

ISBN: 978-3-319-02392-2